arXiv:2402.04233 / A&A accepted

JWST reveals a high fraction of disk breaks at $1 \leq z \leq 3$

Dewang Xu[1,2] and Si-Yue Yu[3]⋆

[1] Department of Astronomy, Peking University, 5 Yiheyuan Road, Haidian District, Beijing, 100871, China
[2] The Kavli Institute for Astronomy and Astrophysics, Peking University, 5 Yiheyuan Road, Haidian District, Beijing, 100871, China
[3] Max-Planck-Institut für Radioastronomie, Auf dem Hügel 69, 53121 Bonn, Germany
e-mail: phyyueyu@gmail.com, syu@mpifr-bonn.mpg.de

Disk Break:

- 3 types in radial profile of disk galaxies (Fig 2)
- Type I : single exponential
- Type II : has steeper profile outside
  Possibly caused by threshold in molecular surface density, radial migration by bar or spirals, or disk instabilities
- Type III : has shallower profile outside
  Merger? Tidal disturbance? Confusion with a stellar halo? Star formation due to gas accretion?

JWST enables us to trace the stellar distribution of galaxies at z=1–3

CEERS Data :

- Z=1–3, $M > 10^{10}\ M_{\odot}$ SFGs
- F356W morphology (axis ratio > 0.5, $R_{50} > 2\times FWHM$)
- 247 galaxies. 42% barred
- Classification
  - Type I, II, III
  - Type IIi, IIo for barred galaxies (break inside bar our outside), but treat Iio as II

Result

- f_I=12.6%, f_II=56.7%, fIIi=4.9%, f_III=34.8%
  : Basically consistent with local results (Fig 3)
- Correlation with physical properties
  - Concentration index correlates with f_II and f_III
  - Weak correlation with U–V color or stellar mass
  - Same trend as local
- Not only the disk structures (spirals and bars, e.g. Fudammoto+22), the disk break is already established in the early universe

Discussions

- Simulation predicts that bar-driven radial migration is expected to leads to Rbrk/Rbar=2–3: consistent with observations ⇔ however, it takes few Gys
- Disk instability may also lead to a break, by flinging out materials

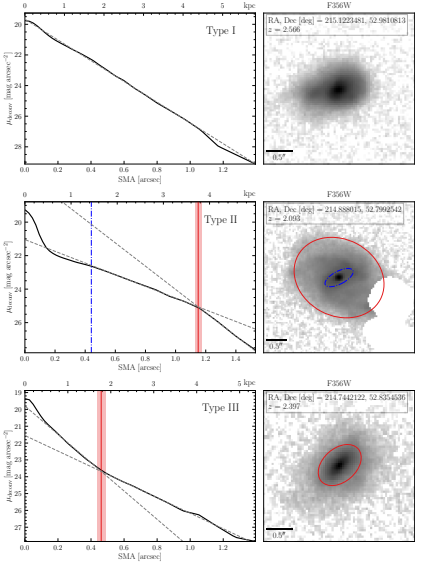

Fig. 2. Classification of the deconvolved disk profiles into three types: Type I (exponential; top), Type II (down-bending; middle), and Type III (up-bending; bottom). The left panels plot the deconvolved surface brightness profiles as a function of semi-major axis (SMA) extracted from deconvolved images. In these, the blue dashed-point line marks the measured bar radius (if present), and the solid red line indicates the identified disk break radius. The dashed lines represent the best-fit exponential functions. On the right, the panels display the deconvolved F356W-band images, with overplotted ellipses corresponding to the bar radius (if present) and disk break radius in the same line styles as in the left panels.

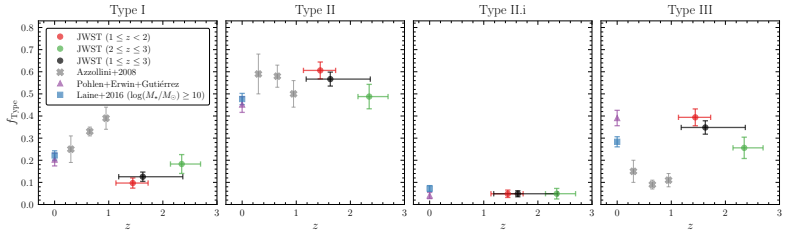

Fig. 3. Comparison of our derived fractions of Type I, Type II, Type II.i, and Type III profiles with those in previous studies. Our results are calculated in three redshift bins and are marked by points positioned at the median redshift. Results derived from the combined data of studies Pohlen & Trujillo (2006), Erwin et al. (2008), and Gutiérrez et al. (2011) in the same series are marked as blue squares; those reported in Laine et al. (2014) are marked by purple triangles. Results based on HST reported in Azzollini et al. (2008) are shown by grey crosses. Error bars associated with the symbols denote the statistical uncertainties.

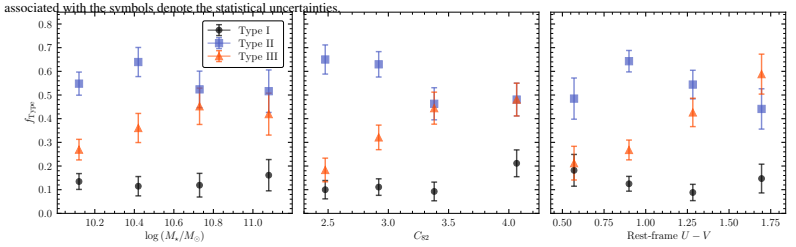

Fig. 4. Dependence of the factions of profile types on stellar mass (left), concentration index C_{82} (middle), and rest-frame color $U - V$ (right).

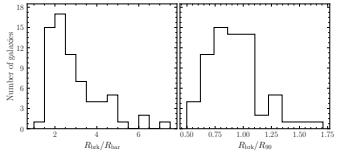

Fig. 5. Distribution of the ratio of Type II break radius ($R_{\rm brk}$) to bar radius ($R_{\rm bar}$) on the left and the ratio of $R_{\rm brk}$ to R_{90} on the right.